Supporting Information

Stable Cycle Performance of Phosphorus Negative Electrode in Lithium-Ion Batteries Derived From Ionic Liquid Electrolytes

Shubham Kaushik, Kazuhiko Matsumoto, Rika Hagiwara*

Graduate School of Energy Science, Kyoto University, Sakyo-ku, Kyoto 606-8501, Japan

*Corresponding Author E-mail Address: k-matsumoto@energy.kyoto-u.ac.jp

Table S1 EIS fitting parameters (R_1, R_2, R_3, R_4, Q_2, Q_3, a_2, a_3, and a_4) during charge-discharge cycling for the Li|P/AB half-cell (1st, 3rd, and 10th cycle) using Org_{PF6}, Org_{FSA}, Org_{FEC}, and $IL_{2:8}$ (see Figure S6(c-f) for the spectra).

Electrolyte		Resistance (Ω)				CPE (F $s^{(a-1)}$)					
	Cycle	R_1	R_2	R_3	R_4	Q_2	a_2	Q_3	a_3	Q_4	a_4
half-cell Li|P/AB	1	9.76	3.69	13.75	0.97	6.92×10^{-6}	0.944	0.11×10^{-3}	0.804	3.78×10^{-3}	0.978
Org_{PF6}	3	6.34	10.16	1.53	1.08	0.24×10^{-3}	0.619	6.57×10^{-3}	0.983	0.22×10^{-3}	0.771
	10	5.09	17.08	1.78	0.42	0.28×10^{-3}	0.598	0.32×10^{-3}	1.000	0.14×10^{-2}	0.495
half-cell Li|P/AB	1	25.48	9.38	15.33	0.07	0.43×10^{-3}	0.560	0.24×10^{-3}	0.652	7.14×10^{-3}	0.875
Org_{FSA}	3	22.40	7.01	14.15	2.29	1.04×10^{-3}	0.550	0.25×10^{-3}	0.622	9.54×10^{-2}	0.883
	10	33.49	6.45	22.56	20.42	8.89×10^{-5}	0.996	0.14×10^{-3}	0.659	0.74×10^{-6}	0.865
half-cell Li|P/AB	1	5.60	1.04	10.16	2.45	2.74×10^{-5}	0.329	0.23×10^{-3}	0.634	4.30×10^{-2}	0.512
Org_{FEC}	3	6.68	0.91	5.91	2.39	2.21×10^{-5}	0.935	0.13×10^{-3}	0.697	3.90×10^{-2}	0.318
	10	7.13	0.64	8.06	1.58	6.19×10^{-5}	0.727	2.45×10^{-3}	0.563	5.23×10^{-3}	0.564
half-cell Li|P/AB	1	10.84	3.88	0.91	0.25	4.57×10^{-5}	0.835	0.30×10^{-3}	0.493	0.88×10^{-3}	0.558
$IL_{2:8}$	3	1.58	3.51	4.23	0.00	8.45×10^{-5}	0.776	2.20×10^{-5}	0.012	9.94×10^{-2}	0.016
	10	4.76	5.31	0.99	1.52	1.91×10^{-5}	0.845	7.81×10^{-3}	0.952	1.95×10^{-2}	0.449

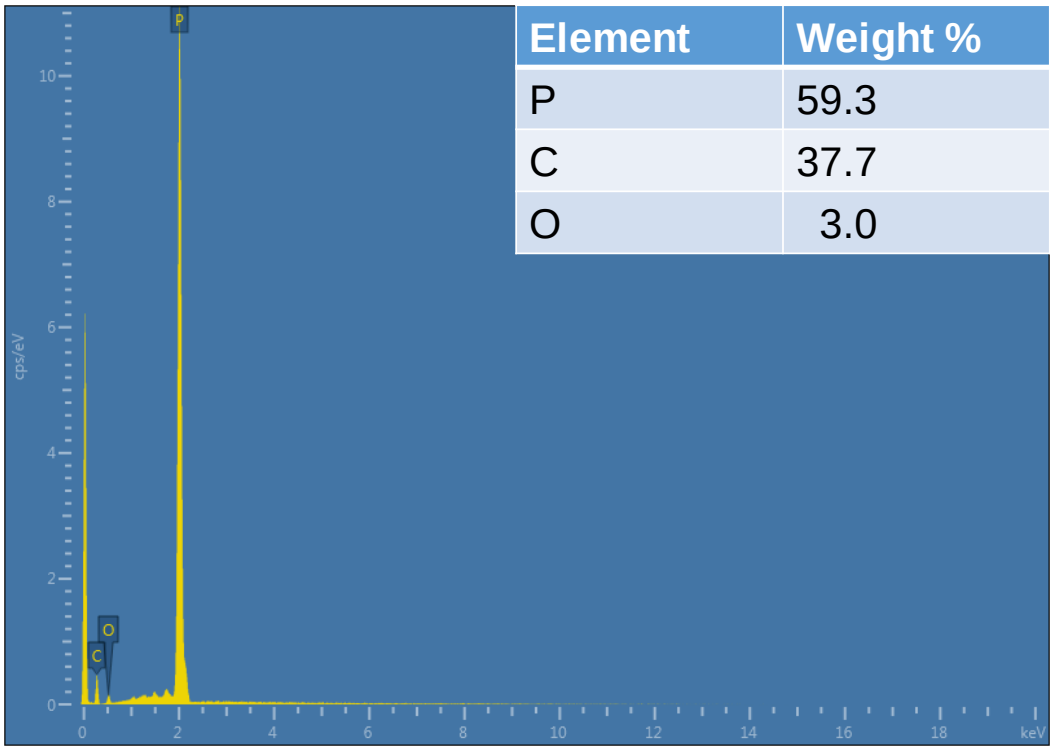

Element	Weight %
P	59.3
C	37.7
O	3.0

Figure S1. The EDX spectrum of the P/AB powder prepared by high-energy ball milling of red P and AB (6:4 in weight) at 900 rpm for 3 h. The resulting elemental compositions are summarized in the inset table.

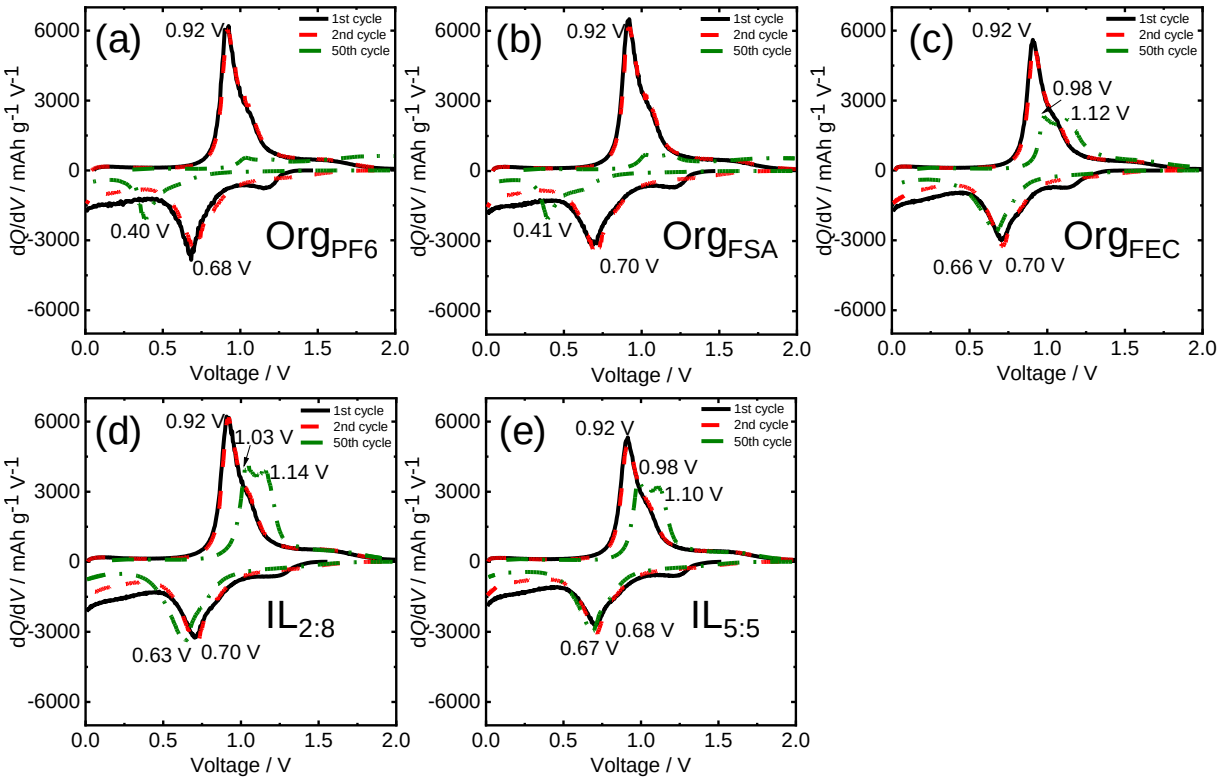

Figure S2. The d*Q*/d*V* plots obtained from the charge-discharge curves of the Li|P/AB half cells using (a) Org_{PF6}, (b) Org_{FSA}, (c) Org_{FEC}, (d) $IL_{2:8}$, and (e) $IL_{5:5}$. The corresponding charge-discharge curves are shown in Figure 2. Current density = 250 mA g^{-1} (1-3 cycles) and 500 mA g^{-1} (4-50 cycles) and cut-off voltage = 0.005–2.0 V. The capacity is calculated based on the weight of the P/AB composite.

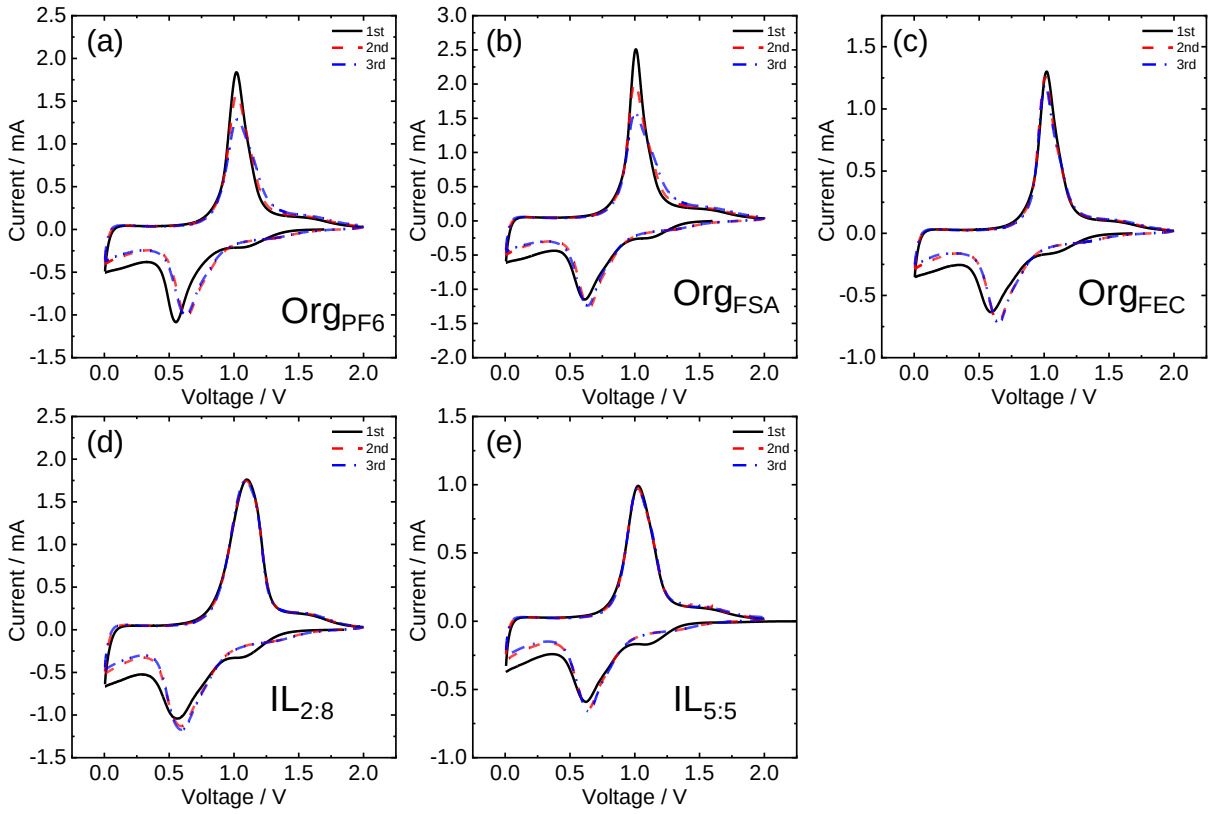

Figure S3. Cyclic voltammograms of the Li|P/AB cells during the first three cycles using (a) Org_{PF6}, (b) Org_{FSA}, (c) Org_{FEC}, (d) $IL_{2:8}$, and (e) $IL_{5:5}$. Scan rate = 0.1 mV s^{-1}; cut-off voltage = 0.005–2.0 V.

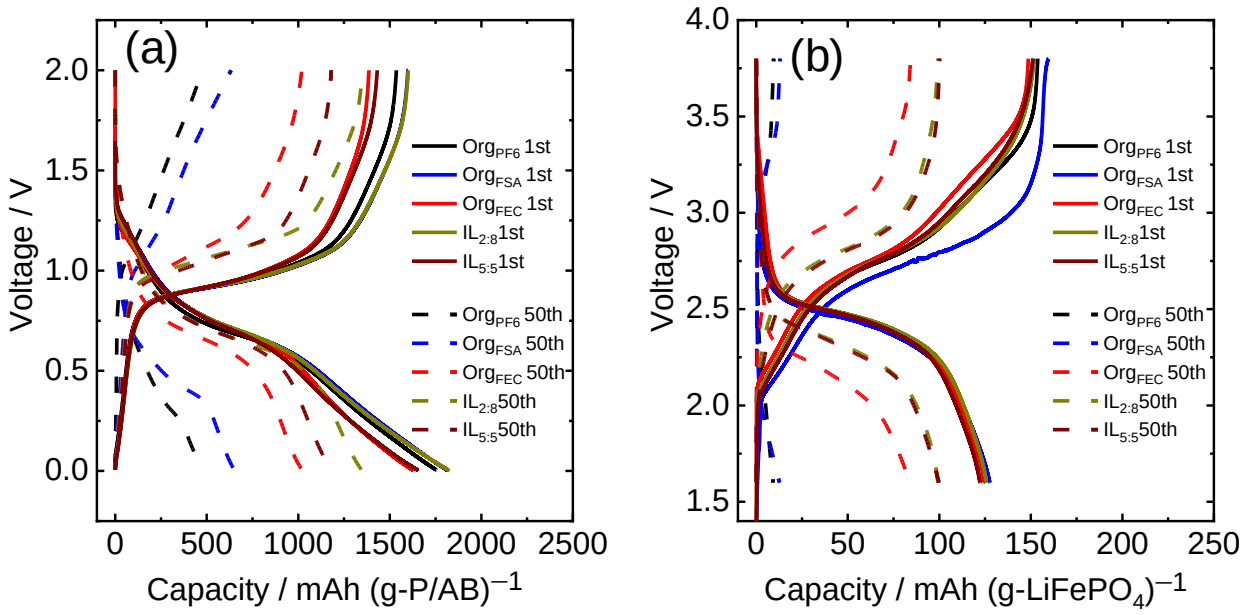

Figure S4. Galvanostatic charge-discharge curves of the (a) Li|P/AB half cells (current density = 250 mA g-(P/AB)$^{-1}$ for 1st cycle and 500 mA g-(P/AB)$^{-1}$ for 50th cycle; cut-off voltage = 0.005–2.0 V) and (b) P/AB|$LiFePO_4$ full cells (1st and 50th cycle) using Org_{PF6}, Org_{FSA}, Org_{FEC}, $IL_{2:8}$, and $IL_{5:5}$ electrolytes (current density = 16 mA g-($LiFePO_4$)$^{-1}$ for the 1st cycle and 80 mA g-($LiFePO_4$)$^{-1}$ for the 50th cycle; cut-off voltage = 1.6–3.8 V). The curves at the 1st and 50th cycles are shown in continuous and dashed lines, respectively, with the same color.

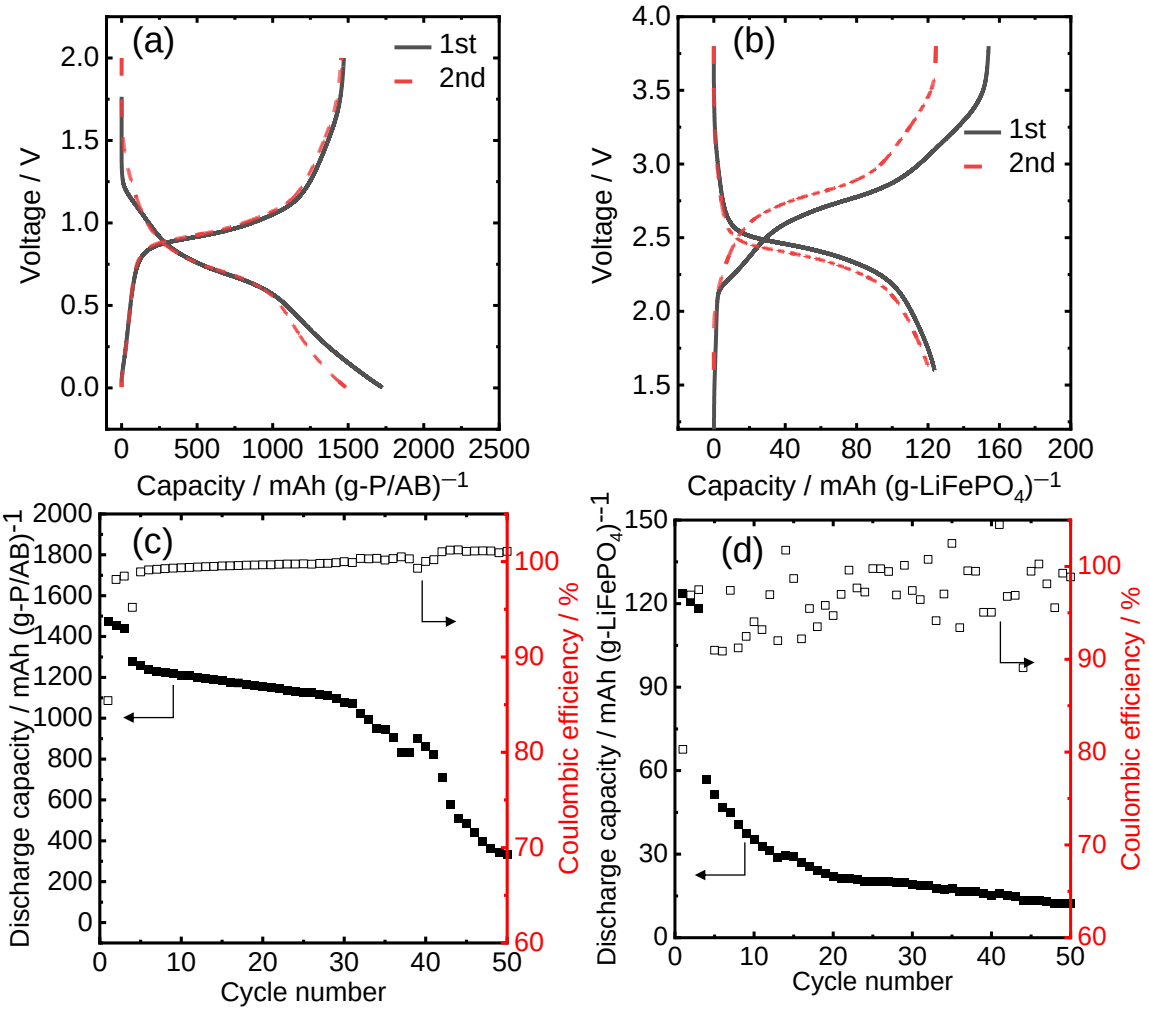

Figure S5. Electrochemical performance of Li|P/AB half cells and P/AB|$LiFePO_4$ full cells using 1 M Li[PF_6] in EC:DMC 3 wt% FEC. Galvanostatic charge-discharge curves of the (a) Li|P/AB half cells (current density = 250 mA g-(P/AB)$^{-1}$; cut-off voltage = 0.005–2.0 V) and (b) P/AB|$LiFePO_4$ full cells, (current density = 16 mA g-($LiFePO_4$)$^{-1}$; cut-off voltage = 1.6–3.8 V). Cycle test of the (c) Li|P/AB half cells (Current density: 1-3 cycles = 250 mA (g-P/AB)$^{-1}$, 4-50 cycles = 500 mA (g-P/AB)$^{-1}$; cut-off voltage = 0.005–2.0 V) and (d) P/AB|$LiFePO_4$ full cells, (Current density: 1-3 cycles = 16 mA (g-$LiFePO_4$)$^{-1}$, 4-50 cycles = 80 mA (g-$LiFePO_4$)$^{-1}$; cut-off voltage = 1.6–3.8 V).

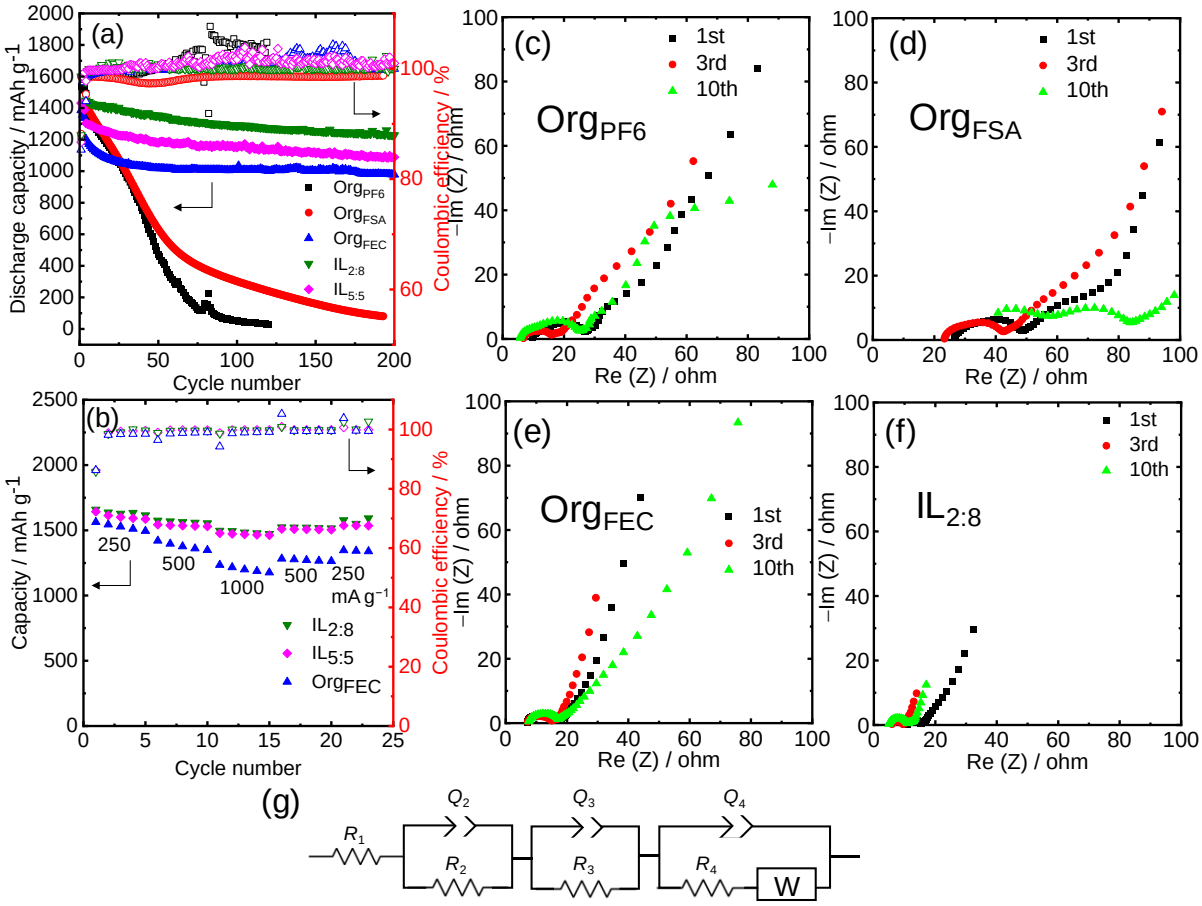

Figure S6. Electrochemical performance of the Li|P/AB half cell and the results of EIS tests during cycling. (a) Cycle performance with Org_{PF6}, Org_{FSA}, Org_{FEC}, $IL_{2:8}$, and $IL_{5:5}$ (Current density: 1-3 cycles = 250 mA $(g\text{-P/AB})^{-1}$, 4-200 cycles = 500 mA $(g\text{-P/AB})^{-1}$; cut-off voltage = 0.005–2.0 V). (b) Rate performance with Org_{FEC}, $IL_{2:8}$ and $IL_{5:5}$ (Current density: 250–1000 mA $(g\text{-P/AB})^{-1}$; cut-off voltage = 0.005–2.0 V). Nyquist plots with (c) Org_{PF6}, (d) Org_{FSA}, (e) Org_{FEC}, and (f) $IL_{2:8}$. EIS was measured at 0.5 V in the charging step of the 2nd, 4th and 11th cycle. (g) Equivalent circuit used for fitting all the EIS Nyquist plots (see Table S1 for the fitted parameters).

Discussion related to Figure S6

In the half-cell cycle test (Figure S6a), capacity fades quickly with Org_{PF6} and Org_{FSA}. The capacity retention improves after adding FEC additive retaining 81.2 % capacity after 200 cycles. Among these organic electrolytes, Org_{PF6} exhibits Coulombic efficiencies over 100 %, owing to active material pulverization resulting in electrolyte decomposition, which is in contrast to the case of Org_{FSA} whose Coulombic efficiencies are kept below 100 %. Both the $IL_{2:8}$ and $IL_{5:5}$ provide high capacity retentions of 84.7 and 82.9 % after 200 cycles with an average Coulombic efficiencies of 100 %. This high capacity retention facilitated by the use of IL electrolytes is unprecedented for phosphorus-based materials for LIBs without employing any complicated fabrication. Figure S6b

shows similar rate capability with $IL_{2:8}$ and $IL_{5:5}$, displaying 1473 and 1463 mAh g^{-1} at 1000 mA g^{-1}. Rate capability with Org_{FEC} is slightly inferior to those with IL electrolytes (1176 mAh g^{-1} at 1000 mA g^{-1}). Figure S6 (c-f) shows Nyquist plots of the Li|P/AB (1st, 3rd and 10th cycle) half cell using (a) Org_{PF6}, (b) Org_{FSA}, (c) Org_{FEC}, and (d) $IL_{2:8}$, respectively. The EIS Nyquist plots were fitted using the equivalent circuit shown in Figure S6g and the fitted parameters are listed in Table S1. The circuit consists of four resistances R_1, R_2, R_3, R_4, and Warburg resistance at low frequency, where R_1 represents the bulk resistance, R_2 denotes the SEI layer resistance at high characteristic frequency (>4000 Hz), and R_3 and R_4 corresponds to the interfacial resistance at medium frequency range (1–500 Hz). Two resistances are used for interfacial behavior for better fitting purpose. In half-cell EIS spectra of Org_{PF6}, Org_{FSA}, and Org_{FEC}, the interfacial resistance decreased after the 3rd cycle (Org_{PF6}: R_2 = 10.16, R_3 = 1.53, R_4 = 1.08 ohm; Org_{FSA}: R_2 = 7.01, R_3 = 14.15, R_4 = 2.29 ohm; Org_{FEC}: R_2 = 0.91, R_3 = 5.91, R_4 = 2.39 ohm) but increased after 10th cycle (Org_{PF6}: R_2 = 17.08, R_3 = 1.78, R_4 = 0.42 ohm; Org_{FSA}: R_2 = 6.45, R_3 = 22.56, R_4 = 20.42 ohm; Org_{FEC}: R_2 = 0.64, R_3 = 8.06, R_4 = 1.58 ohm), respectively as compared to 1st cycle (Org_{PF6}: R_2 = 3.69, R_3 = 13.75, R_4 = 0.97 ohm; Org_{FSA}: R_2 = 9.38, R_3 = 15.33, R_4 = 0.07 ohm; Org_{FEC}: R_2 = 0.64, R_3 = 8.06, R_4 = 1.58 ohm), whereas, a constant decrease till 10th cycle was observed $IL_{2:8}$.

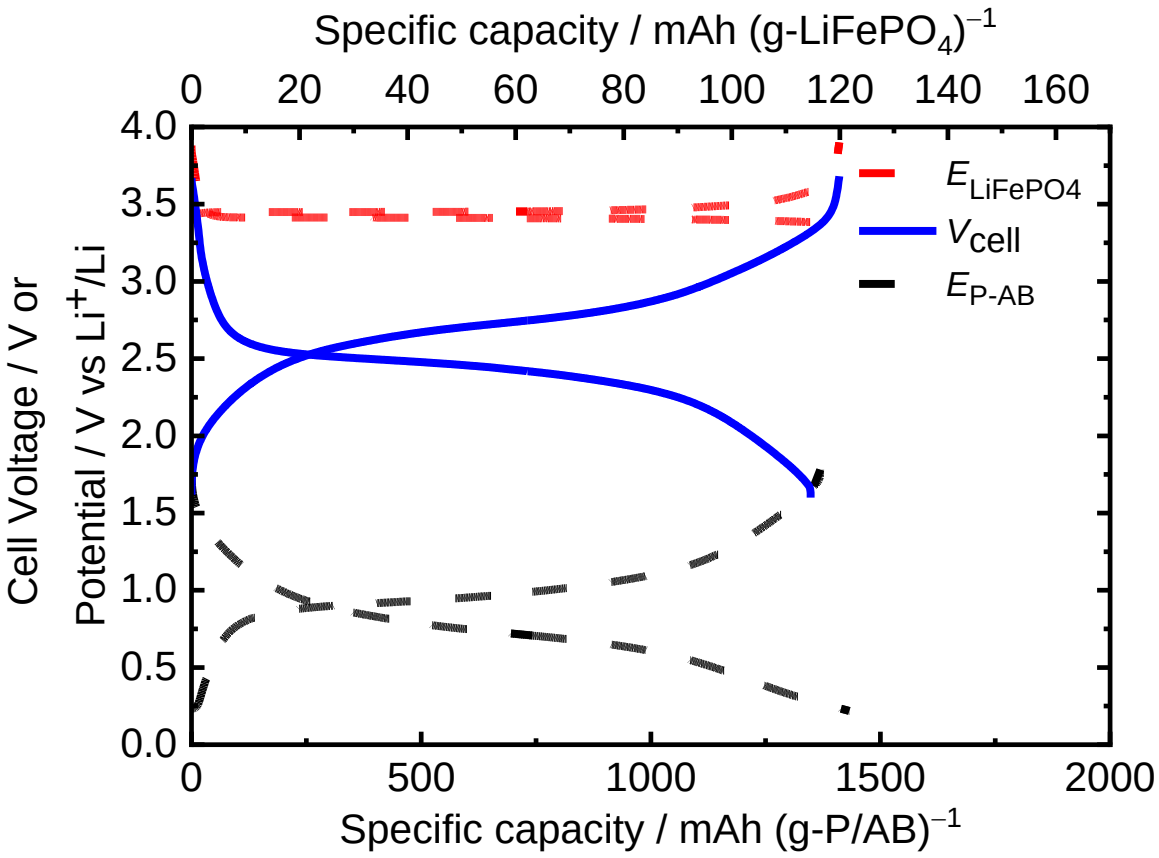

Figure S7. First cycle galvanostatic charge-discharge curves of the P/AB|$LiFePO_4$ full-cell with $IL_{2:8}$ in a three-electrode setup. Current density = 16 mA g-$(LiFePO_4)^{-1}$. The legends, V_{Cell}, $E_{LiFePO4}$, and $E_{P\text{-}AB}$, denote the cell voltage and the potentials of the $LiFePO_4$ positive and P/AB negative electrodes, respectively.

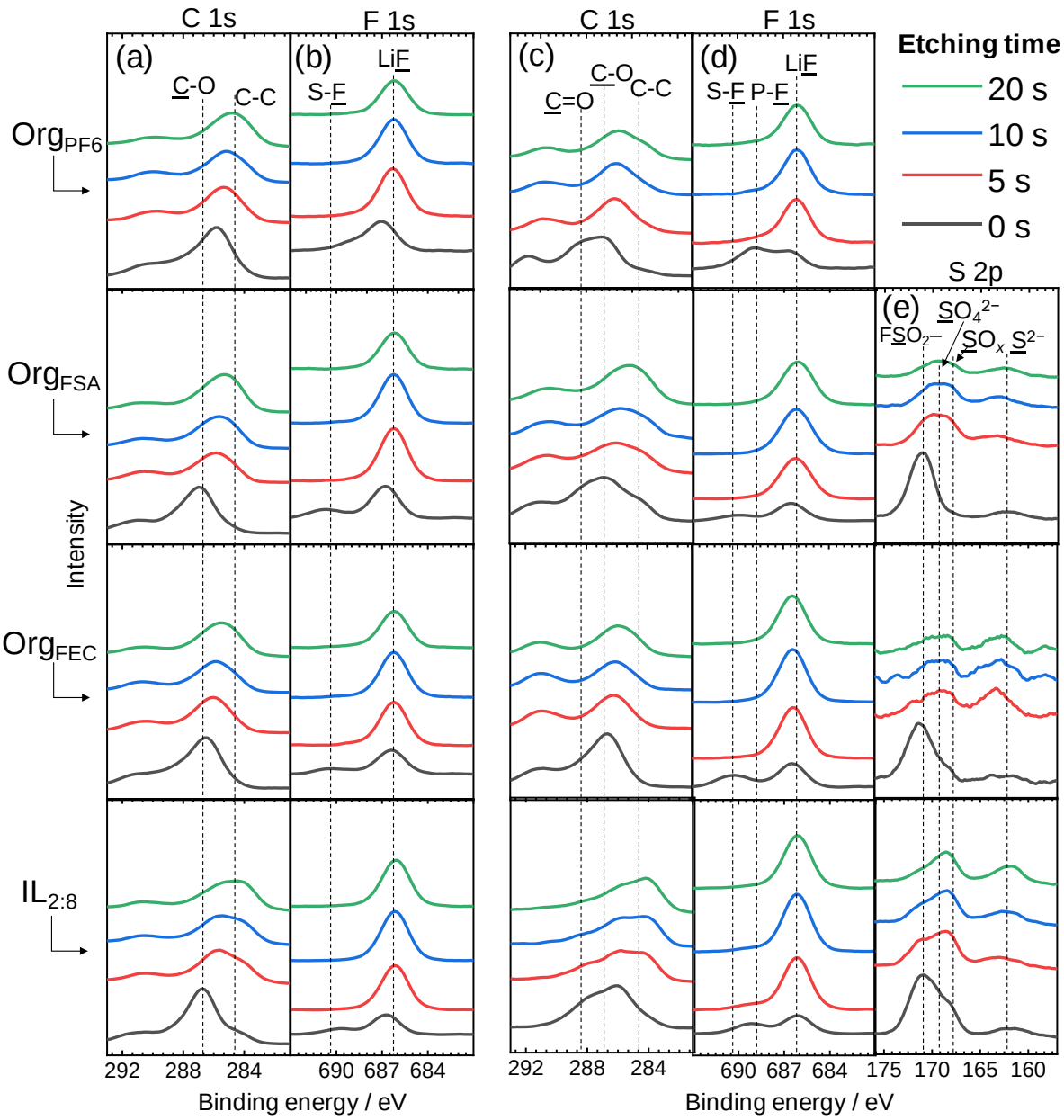

Figure S8. XPS spectra of the P/AB electrode with Ar etching after (a,b) 1st cycle and (c-e) 50th cycle in the C 1s, F 1s and S 2p regions, respectively, using Org_{PF6}, Org_{FSA}, Org_{FEC} and $IL_{2:8}$ electrolytes in the 1st, 2nd, 3rd, and 4th rows respectively.

Discussion related to Figure S8

Figure S8a shows the C 1s spectra after 0, 5, 10, and 20-second etching. The surface without etching is mostly covered by C–O species as denoted by a peak at 286.7 eV [1]. Just 5-second etching results in peak shifting to the lower binding energy and C–C (284.6 eV) species are present in different concentrations according to the electrolyte decomposition. The F 1s spectra (Figure S8b) predominantly consist of LiF (685 eV) in all the electrolytes which is commonly observed in the

SEI layer in LIBs.[2] A small peak of S–F present in F 1s spectrum at 0 s was also confirmed in the S 2p spectrum, which indicates the reaction of F from FSA^- decomposition with organic components. After 50 cycles, further decomposition of electrolytes can be observed. In the C 1s spectra (Figure S8c), a shoulder at 288 eV related to C=O can be observed in Org_{PF6}, Org_{FSA}, and $IL_{2:8}$ but not in Org_{FEC}, indicating that decomposition of FEC in the early stage passivated the electrode and prevented decomposition of carbonate solvents. After etching for 5 s, the C=O layer was stripped off in all the cases, but Org_{PF6}, Org_{FSA}, and Org_{FEC} do not show significant changes with further etching. On the other hand, $IL_{2:8}$ shows evolution of C–C peak with increasing etching time. Figure S8d shows the F 1s spectra after 50 cycles for each electrolyte. The spectrum of Org_{PF6} at 0 s shows distinct peaks around 688.5 eV for the P−F bond in $Li_xF_yPO_z$,[3] and around 685 eV for LiF. After 5-second etching, only LiF peak is observed and further etching did not produce any changes. Other F 1s spectra showed C–F bond peak and LiF peak similar to that after 1st cycle at 0 s, and the C–F peak disappears after 5-second etching. In the S 2p spectra after 50 cycles (Figure S8e), Org_{FSA}, and Org_{FEC} show similar spectra to that after 1st cycle, whereas $IL_{2:8}$ shows a relatively stronger peak at a high binding energy compared to that at 1st cycle. However, after etching for 20 s, the peak of S^{2-} is observable, indicating there is a slight increase in the thickness of SEI layer in IL electrolyte after 50 cycles.

Table S2 Binding energies of the chemical species detected in XPS spectra (Figure S8).

Species	**Binding energy / eV**		
	C1s	**F1s**	**S2p**
C–C	284.6	-	-
C–O	286.7	-	-
C=O	288.0	-	-
S–F	-	690.5	171.5
LiF	-	685.0	-
P–F	-	688.5	
FSO_2–		690.5	171.5
SO_4^{2-}	-	-	169.4
S^{2-}	-	-	162.4

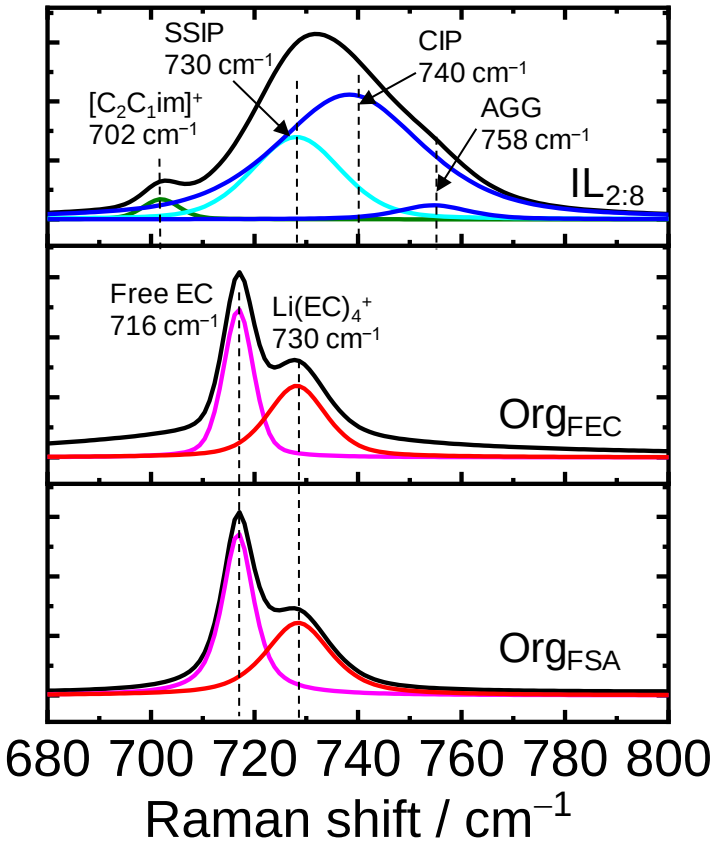

Figure S9. Raman spectra of the Org_{FSA}, Org_{FEC}, and $IL_{2:8}$ electrolytes.

Discussion related to Figure S9:

This range in Raman spectra corresponds to the ring-bending mode of EC and S-N-S bending mode of FSA^- which shift, depending on their coordination states. In Org_{FSA} and Org_{FEC}, the spectrum is deconvoluted into two peaks at 716 and 730 cm^{-1} assigned to the ring-bending vibration of free EC molecule and Li-ion coordinated EC molecule in the form of $Li(EC)_4^+$ (the latter overlaps with the peak for free FSA^- as mentioned below).[4] On the other hand, the Raman spectrum of $IL_{2:8}$ shows four deconvoluted peak at 702, 730, 740, and 758 cm^{-1} correlated to the $C_2C_1im^+$ (at 702 cm^{-1}), free FSA^-(at 730 cm^{-1}), and Li-coordinated FSA^- (contact ion pair (CIP) at 740 and aggregating (AGG) at 758 cm^{-1}), respectively.[5] It should be noted that the absence of the peaks at 740 and 758 cm^{-1} in Org_{FEC} and Org_{FSA} suggest that these electrolytes do not contain the Li ion coordinated by FSA^-. This result suggests that the coordination sphere of Li^+ ion is different in the organic and IL electrolytes; Li^+ is coordinated by solvent molecules decreasing its energy of lower unoccupied molecular orbital in the organic electrolyte, promoting reductive decomposition of solvent. On the other hand, the coordination of Li^+ by FSA^- anion in the IL electrolyte, promotes reductive decomposition of FSA^- anion enabling sulfur based SEI layer formation as observed in XPS result.

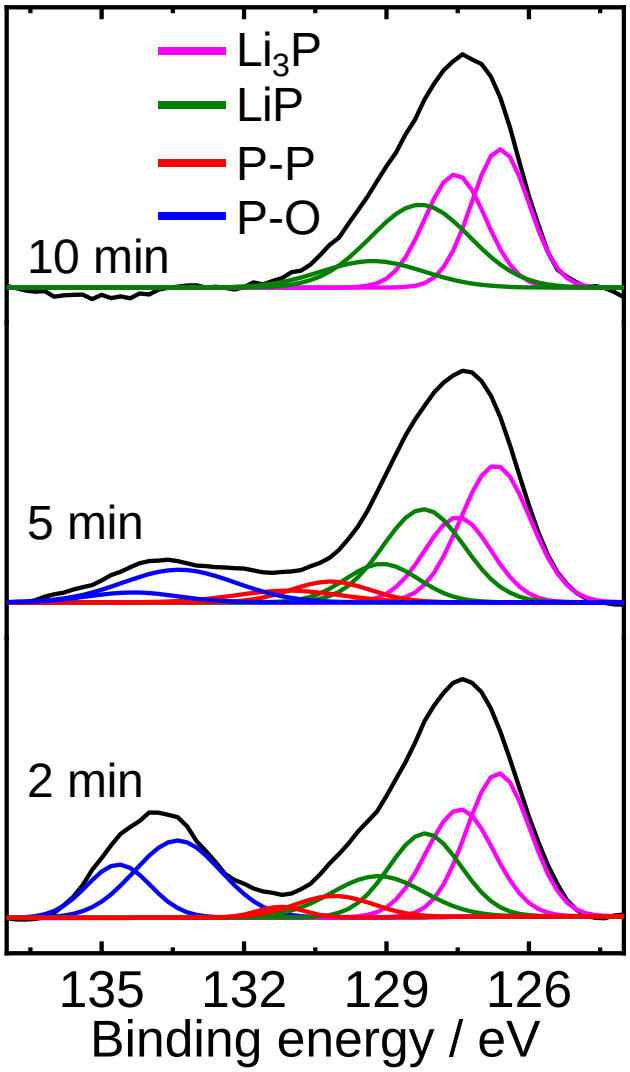

Figure S10. The P 2p XPS of the P/AB electrode after charging to 0.005 V at various Ar etching time of 2, 5 and 10 minutes.

References

1. Shchukarev, A.; Korolkov, D., XPS Study of group IA carbonates. *Open Chemistry* **2004,** *2* (2), 347-362.
2. Hennessy, J.; Nikzad, S., Atomic Layer Deposition of Lithium Fluoride Optical Coatings for the Ultraviolet. *Inorganics* **2018,** *6* (2), 46.
3. Wang, L.; Ma, J.; Wang, C.; Yu, X.; Liu, R.; Jiang, F.; Sun, X.; Du, A.; Zhou, X.; Cui, G., A Novel Bifunctional Self-Stabilized Strategy Enabling 4.6 V LiCoO2 with Excellent Long-Term Cyclability and High-Rate Capability. *Adv. Sci.* **2019,** *6* (12), 1900355.
4. Mukai, K.; Inoue, T.; Kato, Y.; Shirai, S., Superior Low-Temperature Power and Cycle Performances of Na-Ion Battery over Li-Ion Battery. *ACS Omega* **2017,** *2* (3), 864-872.
5. Kerner, M.; Plylahan, N.; Scheers, J.; Johansson, P., Ionic liquid based lithium battery electrolytes: fundamental benefits of utilising both TFSI and FSI anions? *Phys. Chem. Chem. Phys.* **2015,** *17* (29), 19569-19581.